applied sciences

MDPI

Article

Synthesis by Sol–Gel Route of Organic–Inorganic Hybrid Material: Chemical Characterization and In Vitro Release Study

Valentina Petrelli [1], Maria Michela Dell'Anna [1], Piero Mastrorilli [1,*], Veronica Viola [2], Michelina Catauro [2,*] and Antonio D'Angelo [2,3]

[1] Department of Civil, Environmental, Land, Building and Chemical Engineering, Polytechnic University of Bari, Via Edoardo Orabona 4, 70125 Bari, Italy; valentina.petrelli@poliba.it (V.P.); mariamichela.dellanna@poliba.it (M.M.D.)
[2] Department of Engineering, University of Campania "Luigi Vanvitelli", Via Roma n. 29, 81031 Aversa, Italy; veronica.viola@unicampania.it (V.V.); antonio.dangelo@unicampania.it (A.D.)
[3] Department of Environmental, Biological and Pharmaceutical Sciences and Technologies, University of Campania "Luigi Vanvitelli", Via Vivaldi 43, 81100 Caserta, Italy
* Correspondence: pietro.mastrorilli@poliba.it (P.M.); michelina.catauro@unicampania.it (M.C.)

Abstract: Hybrid materials, composed of organic and inorganic components at the nanometer or molecular level, have emerged as a promising material class at the forefront of technological progress. Their potential applications in the biological and medical fields have garnered significant interest, particularly in the context of incorporating antioxidant compounds. This study focuses on the synthesis and characterization of a sol–gel-derived hybrid material, consisting of silica (S), polyethylene glycol (P), and the antioxidant flavonoid quercetin (Q). By varying the concentrations of Q and P, the structural and biological properties of the SPQ hybrid systems were investigated. Structural analysis using Fourier-transform infrared (FT-IR) and solid-state nuclear magnetic resonance (NMR) spectroscopies provided insights into the material composition and morphology, giving information about the interactions between the organic and inorganic phases. Additionally, the in vitro release study revealed a controlled release of quercetin over time, demonstrating that the hybrid materials possess a suitable application for drug delivery.

Keywords: hybrid materials; sol–gel; solid-state NMR; FT-IR; FT-IR deconvolution; drug delivery; quercetin

Citation: Petrelli, V.; Dell'Anna, M.M.; Mastrorilli, P.; Viola, V.; Catauro, M.; D'Angelo, A. Synthesis by Sol–Gel Route of Organic–Inorganic Hybrid Material: Chemical Characterization and In Vitro Release Study. *Appl. Sci.* **2023**, *13*, 8410. https://doi.org/10.3390/app13148410

Academic Editor: Ilaria Cacciotti

Received: 20 June 2023
Revised: 12 July 2023
Accepted: 18 July 2023
Published: 20 July 2023

1. Introduction

Hybrid materials, unlike conventional composites that consist of constituents at the macroscopic level, are materials formed by the synergistic combination of organic and inorganic components at the nanometer or molecular level [1,2]. Today, hybrid materials represent one of the emerging material classes cutting the edge of technological progress [3], which, according to the achieved properties, can be applied to a wide range of fields. Among all the possible applications, hybrid materials can be applied in biological and medical fields when they possess specific interesting characteristics [4–8].

Among the substances of medical and biological interest, there are antioxidant compounds. Antioxidant compounds are a group of molecules that can be found in a variety of foods that help protect cells from damage caused by free radicals [9]. These are highly reactive molecules that are formed as a natural metabolic byproduct, as well as through exposure to environmental toxins, such as tobacco smoke and air pollution [10,11]. Specifically, any molecular species with an unpaired electron in an atomic orbital and the ability to sustain its existence is referred to as a free radical. They act as oxidants or reductants depending on whether they give or take an electron from other molecules [12]. When free radicals accumulate in the body, they can damage cells, reacting with DNA and proteins, and enhance a wide range of health problems, such as cancer and cardiovascular and

neurodegenerative diseases [12,13]. Antioxidants counteract free radicals, preventing cell damage. Several types of antioxidants exist, encompassing vitamins C and E, beta-carotene, selenium, and flavonoids, among others [14].

Among the class of flavonoids, there is quercetin, whose properties have been widely recognized [15]. Quercetin (Q) is known not only for its potent antioxidant features [16], but also for its role in the prevention of inflammation and its ability to support the immune system thanks to its ability to stimulate the production of white blood cells, which are essential for fighting off infections [17,18]. Given its characteristics, quercetin is a compound that could offer many advantages if inserted into a material, especially if the purpose of this material is to be used as a biomaterial [19,20].

For several years, our research group has been actively engaged in studying the incorporation of bioactive molecules into materials using the sol–gel technique. The traditional sol–gel route involves a series of hydrolysis and condensation reactions of sol–gel-reactive alkoxide precursors with water in the presence of a catalyst usually diluted in an appropriate solvent [21,22]. By using this method, the hybrid systems made up of silica (S) and polyethylene glycol (P), namely SP hybrids, have been fully characterized and discussed in [23]. Further, a preliminary investigation on silica (S), polyethylene glycol (P), and quercetin (Q) hybrids (SPQ systems) was also reported in [24]. Even though these studies pointed out the thermal properties, the biocompatibility on eucaryotic cells, and the antimicrobial activity of the synthesized hybrids, a deep investigation of the hybrid chemical properties, as well as of the release of the entrapped drug, needs to be carried out. As a consequence, this study aims to shed new light on the interactions among the organic and inorganic components by the combination of FT-IR and solid-state NMR spectroscopies and to investigate the in vitro release of the used drug. The importance of studying this release is fundamental to obtain an entire overview of the applicability of these systems in biomedical fields [25], especially for bone repair, to which glass-based hybrid materials have mainly been applied [26].

The SPQ hybrid systems, the object of this study, were synthesized with different percentages of P (from 0 to 50 wt%) and Q (from 0 to 20 wt%), without changing the synthesis procedure already reported in [24].

2. Materials and Methods

2.1. Sol–Gel Synthesis

The sol–gel method was performed to obtain silica hybrid materials with different percentages of P and Q as summarized in Table 1.

Table 1. Sample labels and names.

Sample	Polyethylene Glycol (P, wt% in Relation to SiO_2 Matrix)	Quercetin (Q, wt% in Relation to SiO_2 Matrix)
SQ5	0	5
SQ10	0	10
SQ15	0	15
SQ20	0	20
SP6Q5	6	5
SP6Q10	6	10
SP6Q15	6	15
SP6Q20	6	20
SP12Q5	12	5
SP12Q10	12	10
SP12Q15	12	15
SP12Q20	12	20
SP24Q5	24	5
SP24Q10	24	10
SP24Q15	24	15
SP24Q20	24	20

Table 1. *Cont.*

Sample	Polyethylene Glycol (P, wt% in Relation to SiO_2 Matrix)	Quercetin (Q, wt% in Relation to SiO_2 Matrix)
SP50Q5	50	5
SP50Q10	50	10
SP50Q15	50	15
SP50Q20	50	20

Tetraethyl orthosilicate (TEOS, $Si(OC_2H_5)_4$, Sigma-Aldrich, Darmstadt, Germany) was used as the inorganic metal alkoxide precursor, whereas quercetin (Q, Sigma-Aldrich) and polyethylene glycol (P, MW = 400, Sigma-Aldrich) were used as organic phases. The inorganic precursor was mixed under continuous stirring with pure ethanol (EtOH, 99%, Sigma-Aldrich) and MilliQ water following the molar ratio of EtOH:TEOS:H_2O = 6:1:4. Concurrently, P and Q sols were prepared by dissolving different amounts of the organic components into pure EtOH. Q and P sols were mixed drop by drop with TEOS-based solutions under continuous stirring at room temperature (27 °C). Finally, nitric acid (HNO_3, 65%, Sigma-Aldrich) was added to the solutions with a molar ratio of HNO_3: TEOS = 0.6 to speed up the reactions [27,28]. After gelation occurrences (8 days), to allow for the removal of the residual solvent, the obtained wet gels were dried at 50 °C for 24 h. The whole adopted sol–gel procedure is shown in Figure 1, while a focus on the reactions is reported in Figure 2. Following the reaction mechanisms found in the literature [29–31], the acid-catalyzed hydrolysis reaction was based on SN_2 mechanisms (Figure 2B).

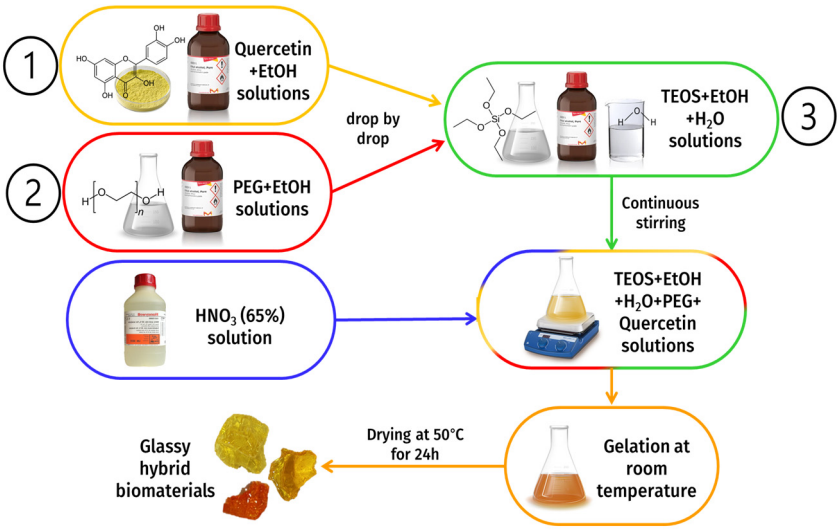

Figure 1. Synthesis of the hybrid materials. (1) quercetin-based (from 5 to 20 wt% with respect to the silica content); (2) polyethylene glycol-based sols (from 6 to 50 wt% with respect to the silica content); (3) TEOS-based sols to be mixed with sols 1 and 2.

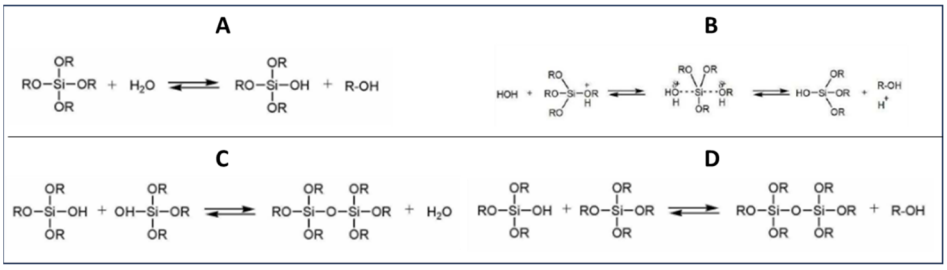

Figure 2. Sol–gel reaction mechanism when the precursor is TEOS (R= -CH_2CH_3). (**A**) Hydrolysis reaction; (**B**) acid-catalyzed hydrolysis reaction with SN_2 mechanism; (**C**) water condensation; and (**D**) alcohol condensation.

2.2. Fourier-Transform Infrared Spectroscopy

FT-IR analysis was conducted to investigate the chemical compositions of the materials and examine the interactions between their components. The FT-IR spectra were collected in the 400–4000 cm^{-1} range with a resolution of 2 cm^{-1} (60 scans) using a Prestige21 Shimadzu (Milan, Italy) spectrometer equipped with a DTGS KBr detector (deuterated triglycine sulphate with potassium bromide windows). To prepare the samples, 2.00 mg of each material was mixed with dried KBr powder (198.00 mg) and compressed into small disks weighing 200.00 mg. The FT-IR spectra were processed using IR Solution and Origin 8 software. The main peak in the 1650–750 cm^{-1} range was deconvoluted using the Multiple Peak Fit tool in Origin 8 software, employing a Gaussian function.

2.3. Nuclear Magnetic Resonance Spectroscopy

Solid-state CP/MAS NMR analysis was performed on a Bruker Avance I 400 spectrometer (operating at a frequency of 100.6 MHz for ^{13}C and 79.4 MHz for ^{29}Si), using a 4.0 mm HX MAS probe at 298 K. Samples (ca. 80 mg) were packed in 4 mm zirconia rotors and spun under airflow at 14.5 kHz ($^{1}H-^{13}C$ CP/MAS) or 10.0 kHz ($^{1}H-^{29}Si$ CP/MAS). $^{1}H-^{13}C$ CP/MAS NMR experiments were acquired using a 3.25 μs proton 148 $\pi/2$ pulse length, a ν_{CP} of 55.0 kHz, a ν_{dec} of 76.9 kHz, a recycle delay of 4.0 s, and a contact time of 1.0 ms. This contact time is eligible to show only the narrow component of the PEG signal, which corresponded to the amorphous phase [32]. $^{1}H-^{29}Si$ CP/MAS NMR experiments were acquired using a recycle delay of 4.0 s and a contact time of 7.0 ms. A two-pulse phase-modulation (TPPM) decoupling scheme was used for ^{1}H decoupling. Chemical shifts were referenced to $SiMe_4$ (0 ppm) by using the methylene signal of adamantane (δ 38.48) as a secondary reference for ^{13}C and tetramethylsilane (δ 0.00) for ^{29}Si. The condensation degree (c.d.) of silica in the hybrid materials [33] was assessed by the following formula:

$$\text{c.d.} = (4 \times Q_4 + 3 \cdot Q_3 + 2 \cdot Q_2)/(4 \times (Q_4 + Q_3 + Q_2)) \quad (1)$$

where Q_2, Q_3, and Q_4 are the integrals of the corresponding Q signal that are due to the $[Si(OSi)_2(OH)_2]$, $[Si(Osi)_3OH]$, and $[Si(OSi)_4]$ units, respectively.

2.4. In Vitro Release

To evaluate the release behavior of the enclosed drug, an in vitro release study was conducted on the hybrid materials. Shimadzu UV mini-1240 was used for the test, and measurements were made at a wavelength of lambda λ 299.0 nm, which corresponds to the maximum absorption of quercetin. The tests were carried out in a simulated body fluid (SBF), which is a fluid mimicking the ion concentration of blood plasma (as reported in Table 2) [34]; it is also useful for predicting hybrids' bioactivity [35,36].

Table 2. Comparison of ion concentration in SFB and blood plasma.

Ion	SBF (mM)	Blood Plasma (mM)
Na^+	142.0	142.0
K^+	5.0	5.0
Mg^{2+}	1.5	1.5
Ca^{2+}	2.5	2.5
Cl^-	103.0	103.0
HCO_3^-	10.0	27.0
HPO_4^{2-}	1.0	1.0
SO_4^{2-}	0.5	0.5

A total of 25 mg of sample powders were mixed with 50 mL of SBF solution (at pH = 7.4) under continuous stirring at 37 °C. The quercetin absorbance measurements were taken in triplicate at t = 0, 0.5, 1, 2, 4, 6, 8, and 24 h, and the results were interpolated to the calibration curve.

The calibration curve, reported in Figure 3, was obtained by measuring the absorbance of standards made in the SBF and establishing a correlation between solution concentrations and absorbance at a length of 299.0 nm, with R^2 = 0.9992. The upper limit was at 50.0 mg/L, while the lower limit was at 5.0 mg/L.

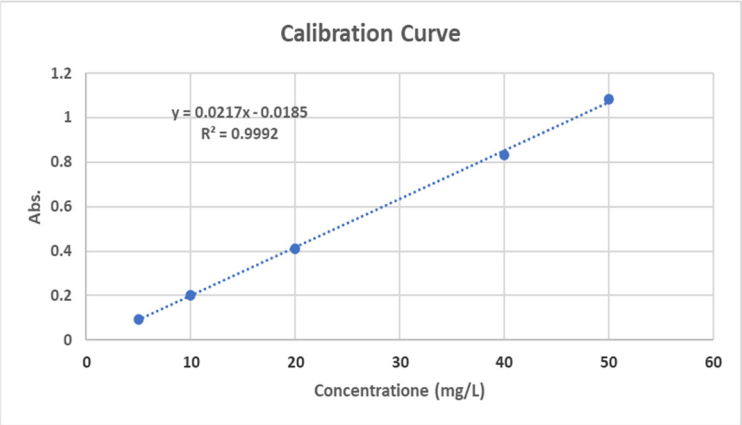

Figure 3. Calibration curve of quercetin extracted from the synthesized SQ20 hybrid system.

3. Results and Discussion

3.1. FT-IR and Deconvolution Study

In our previous work, both the absorption bands and the H-bonds between the organic and inorganic phases have been revealed by FT-IR and Raman spectroscopies [24,37,38]. Moreover, it has also been demonstrated that Q underwent an oxidation phenomenon [38]. Indeed, the quercetin molecule is formed by a carbonyl group in position 4, a double bond between carbons 2 and 3, and five hydroxy groups in positions 3, 5, 7, 3′ and 4′. The hydroxyl groups on the quercetin molecule can be oxidized by nitric acid, resulting in the formation of quinones and decomposition products. This oxidation process leads to a visible color change due to the distinct electronic structures of the newly formed chemical species, which, in turn, can affect the absorption and reflection of light [39,40]. Starting from those results, to better comprehend the influence of the oxidized Q (Qox) and P on the S matrix, the deconvolution of the main absorption band in the range of 1650–750 cm^{-1} (see green rectangle in Figure 4) is reported.

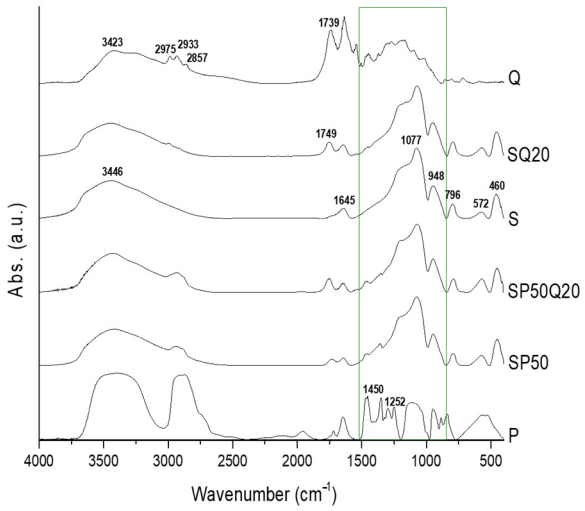

Figure 4. FT-IR spectra of S, Q, P, and hybrid systems.

Deconvoluted spectra (Figure 5A–D) shed light on the main absorption band contributes of both the organic and inorganic components within the hybrids, thus result-

ing in the hypothesis of an interaction between the SiO_2 matrix, polyethylene glycol, and quercetin.

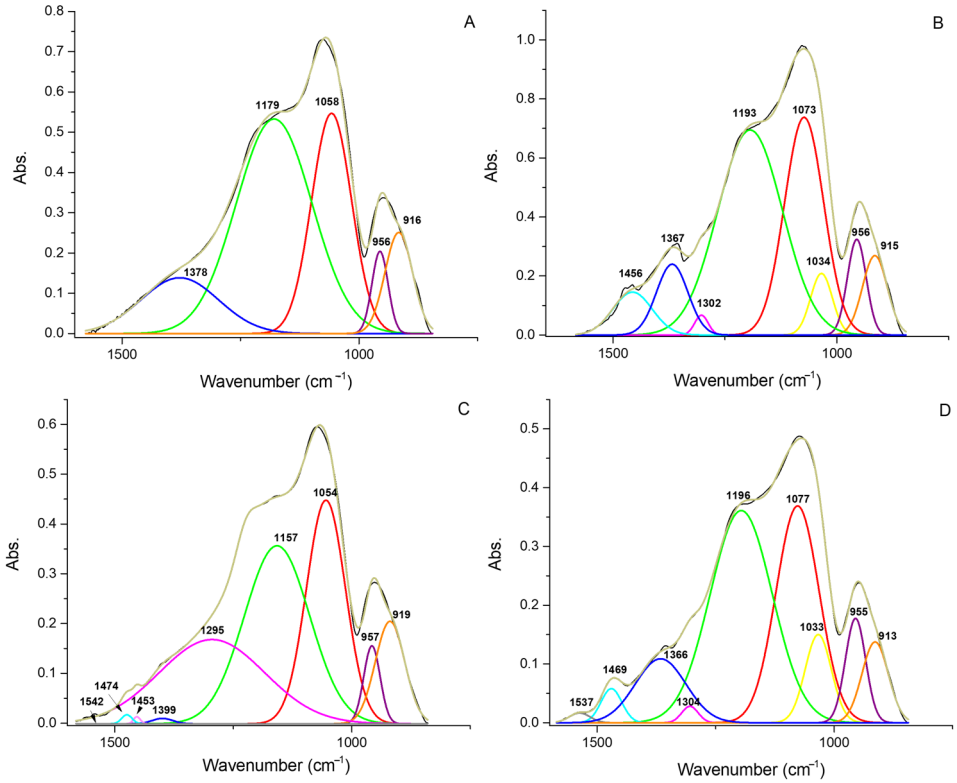

Figure 5. Deconvoluted FT-IR spectrum of (**A**) S; (**B**) SP50; (**C**) SQ20; and (**D**) SP50Q20 in the 1650–750 cm^{-1} range.

In particular, the main absorption bands in the deconvoluted spectrum of the silica (Figure 5A) were detected at 1378, 1179, 1058, 956, and 916 cm^{-1}. The signal at 1378 cm^{-1} could be assigned to the vibration coming from residual ethanol not completely removed from the synthesized SiO_2 matrix [41], whereas the bands at 1179, 1058, 956, and 916 cm^{-1} are typical of the silica matrix [42–44]. In Figure 5A, the Si-O-Si asymmetric stretching vibration (transverse optical mode), attributed to the most dominant band, was detected at 1058 cm^{-1} [45,46], whereas the high-frequency shoulder at 1179 cm^{-1} is assigned to the skeletal Si-O-Si stretching vibration (longitudinal optical mode) [42]. Even if this band is not typically IR active, because of the matrix porosity, this mode does exist, resulting in this visible signal. The absorption bands at 956 and 916 cm^{-1} are due to the Si-O stretching of the surface silanol groups and to the Si-OH bending vibration [47,48], respectively. In the SP50 deconvoluted spectrum (Figure 5B), new absorption bands, centered at 1034, 1224, 1302, 1367, 1456, and 1500 cm^{-1}, are assigned to polyethylene glycol. Indeed, 1500, 1456, and 1367 cm^{-1} are due to the C-H vibrations [49–51], while the new signal at 1034 cm^{-1} may be derived from C-O stretching. The absorption band of C-O stretching is generally located at 1080–1060 cm^{-1} [52], so the observed red shift may be associated with the formation of H-bonds between the PEG oxygens and the silanol groups of the matrix. Indeed, the main skeletal Si-O-Si vibrations (centered at 1179 and 1058 cm^{-1}, in the silica matrix alone) also shifted to higher wavenumbers (1193 and 1073 cm^{-1}, respectively). Furthermore, the silica peak at 1073 cm^{-1} is superimposed on the C-O-H stretching signal [53], generally located at 1080 cm^{-1}, thus enforcing the hypothesis. The influence of the quercetin drug on the FT-IR spectrum of silica is shown in Figure 5C. The new signal at 1224 cm^{-1} could be assigned to the C-O-C aryl ketone vibration of the quercetin [54–56]. According to Silverstein [57], this absorption band is found at 1260 cm^{-1}. The shift at lower wavenumbers could be due to the chemical environment of the silica matrix. Indeed, a shift to lower wavenumbers of the Si-

O-Si vibration was also detected (see the absorption band at 1157 cm^{-1}). The deconvoluted spectrum showed that other new absorption bands have been found at 1474 cm^{-1} and 1399 cm^{-1}, both related to C-H vibrations. Finally, Figure 5D reports the influence of both organic phases on the silica matrix. Both Q and P affect the main Si-O-Si skeletal absorption band, resulting in a shift at higher wavenumbers (from 1179 and 1058 cm^{-1} to 1196 and 1077 cm^{-1}). The signals observed, along with the intensified C-O absorption band (which is more prominent compared to the deconvoluted spectrum of the SP50 hybrid in Figure 5B) at 1033 cm^{-1} and the enhanced intensity of the C-H absorption (represented by a broad peak detected at 1366 cm^{-1}) originating from the organic phases, provide further support for the hypothesis of interactions among all the components within the hybrid materials.

3.2. NMR Study

Figure 6A shows the ^{1}H-^{13}C CP-MAS NMR spectrum of P used in this work, showing three peaks at δ 72.8, δ 70.5, and δ 61.2, attributable to $HOCH_2CH_2$, to the backbone ether carbons, and to $HOCH_2CH_2$, respectively. The FWMH of the peaks is ca. 49 Hz, and their integrals are 2:13.4:2, consistent with the mean molecular weight of 400 da. The ^{1}H-^{13}C CP-MAS NMR spectra of the hybrid systems composed of S, P, and Q show, together with peaks attributable to P, signals at ca. δ 165, δ 58.3, and δ 14.5, attributable to the aerobic oxidation products of quercetin, Qox, whose antioxidant properties have been recently explored by Speisky et al. [40,58]. The ^{1}H-^{13}C CP-MAS NMR spectrum of pure (not oxidized) quercetin is reported in Figure 6B, for comparison.

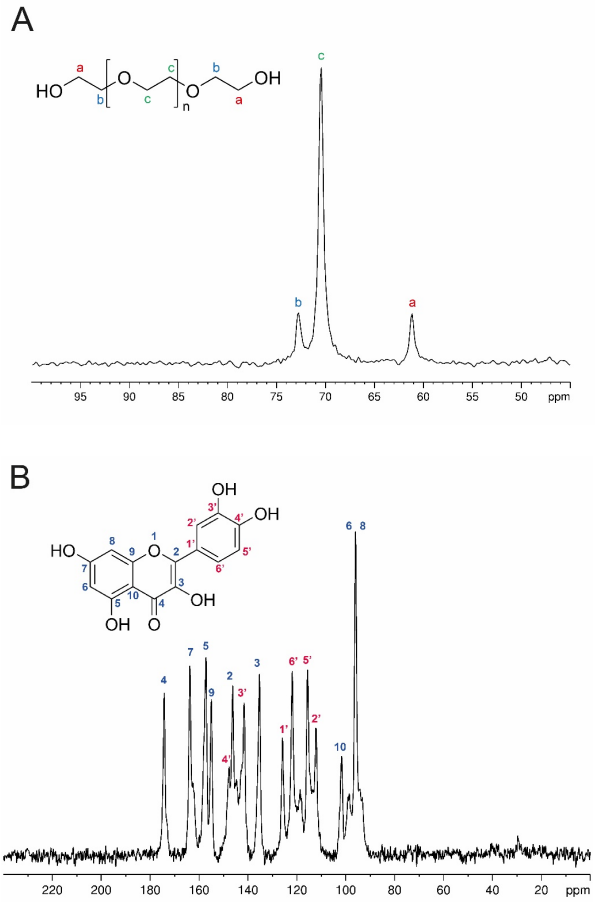

Figure 6. (**A**) ^{1}H-^{13}C CP-MAS NMR spectrum of P; (**B**) ^{1}H-^{13}C CP-MAS NMR spectrum of Q.

As a representative example, Figure 7 shows the ^{1}H-^{13}C CP-MAS NMR spectrum of SP50Q20, while Figure 8 shows the comparison between the ^{1}H-^{13}C CP-MAS NMR spectrum of pure polyethylene glycol with those of the hybrid systems.

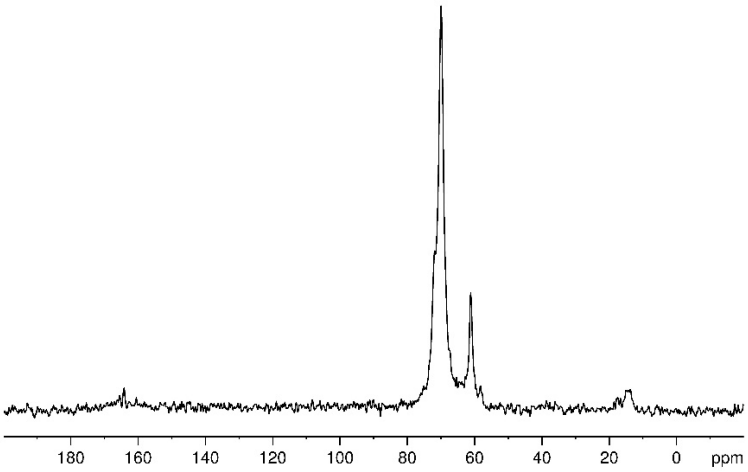

Figure 7. ^{1}H-^{13}C CP-MAS NMR spectrum of SP50Q20.

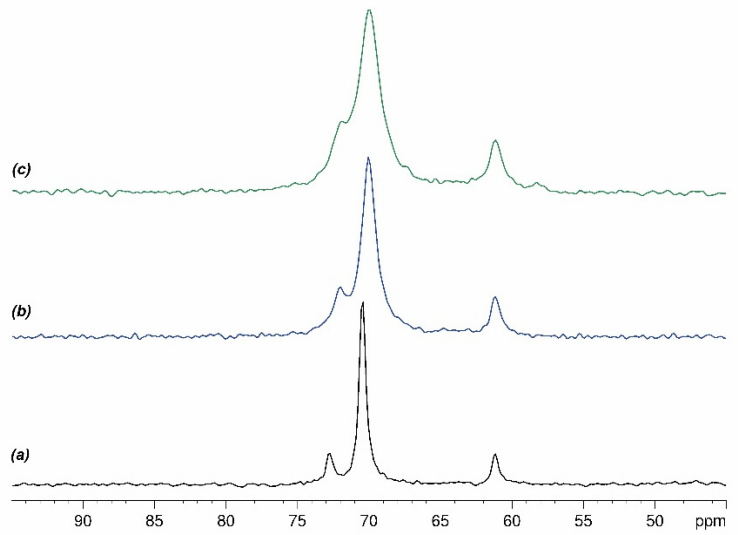

Figure 8. ^{1}H-^{13}C CP-MAS NMR spectra of pure P (**a**); SP50 hybrid system (**b**); SP50Q20 hybrid system (**c**).

It is apparent that SP50Q20 exhibits ^{13}C NMR peaks that are slightly high-field-shifted (δ 71.8, δ 69.9 and δ 61.1) and that the peak due to the backbone carbons shows a larger FWMH (ca. 172 Hz), with respect to pure P. Such features can be attributed to weak interactions between P and SiO_2 and/or Qox. The ^{1}H-^{13}C CP-MAS NMR spectrum of the composite made up of SiO_2 and polyethylene glycol confirms the S and P interactions since a similar peak shift, as observed in SP50Q20, is recorded. However, a weak interaction of Qox cannot be excluded given that the broadness of the ^{13}C NMR peaks in the SP50Q20 sample is larger than that of the SP50 composite (ca. 110 Hz). In order to gain insights into the effect of Qox charge onto the broadness of the P ^{13}C NMR peaks, we prepared hybrid systems containing 5% (SP50Q5), 10% (SP50Q10), and 15% (SP50Q15) of quercetin and recorded their ^{1}H-^{13}C CP-MAS NMR spectra (Figure 9a–d), from which it appears that a higher amount of quercetin results in a larger FWMH.

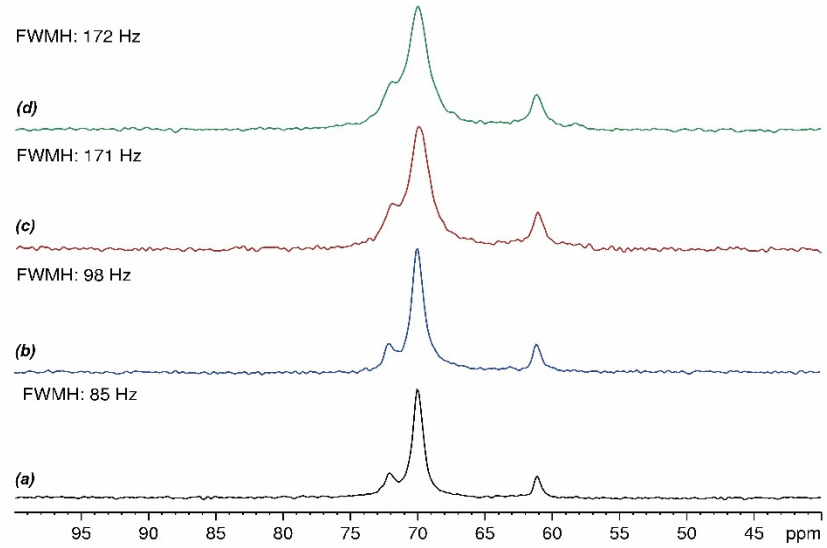

Figure 9. ^{1}H-^{13}C CP-MAS NMR spectra of SP50Q5 (**a**); SP50Q10 (**b**); SP50Q15 (**c**); and SP50Q20 (**d**). The reported FWMH refers to the peak at δ 69.9.

Figure 10 shows the ^{1}H-^{29}Si CP-MAS NMR spectra of S, SP50, and SP50Q20. In this case, all spectra are nearly superimposable, indicating that silicon atoms are not involved in strong interactions with PEG or quercetin. The peaks present in the spectra are at δ–87.5, δ–96.9, and δ–105.7 and are attributable to silicon atoms conventionally denoted as Q_2 [$Si(OSi)_2(OH)_2$], Q_3 [$Si(OSi)_3OH$], and Q_4 [$Si(OSi)_4$] due to bi-, tri-, and tetrabranching units, respectively. The condensation degree of the three samples (76 for SiO_2; 78 for SP50; and 77 for SP50Q20) calculated on the basis of the relative intensity of Q_2, Q_3, and Q_4 peaks [33] is almost identical.

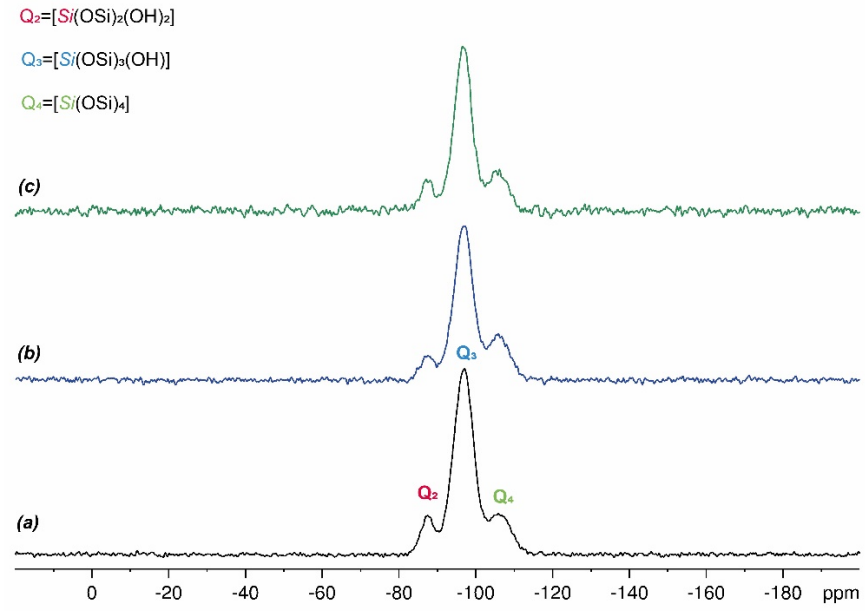

Figure 10. ^{1}H-^{29}Si CP-MAS NMR spectra of S (**a**); SP50 (**b**); and SP50Q20 (**c**).

3.3. Release Study

The results of the oxidized-quercetin-release study for all the systems are shown in Figure 11. The graph in Figure 10a shows how quercetin release varies in the SQ5 and SP(6–50)Q5 systems.

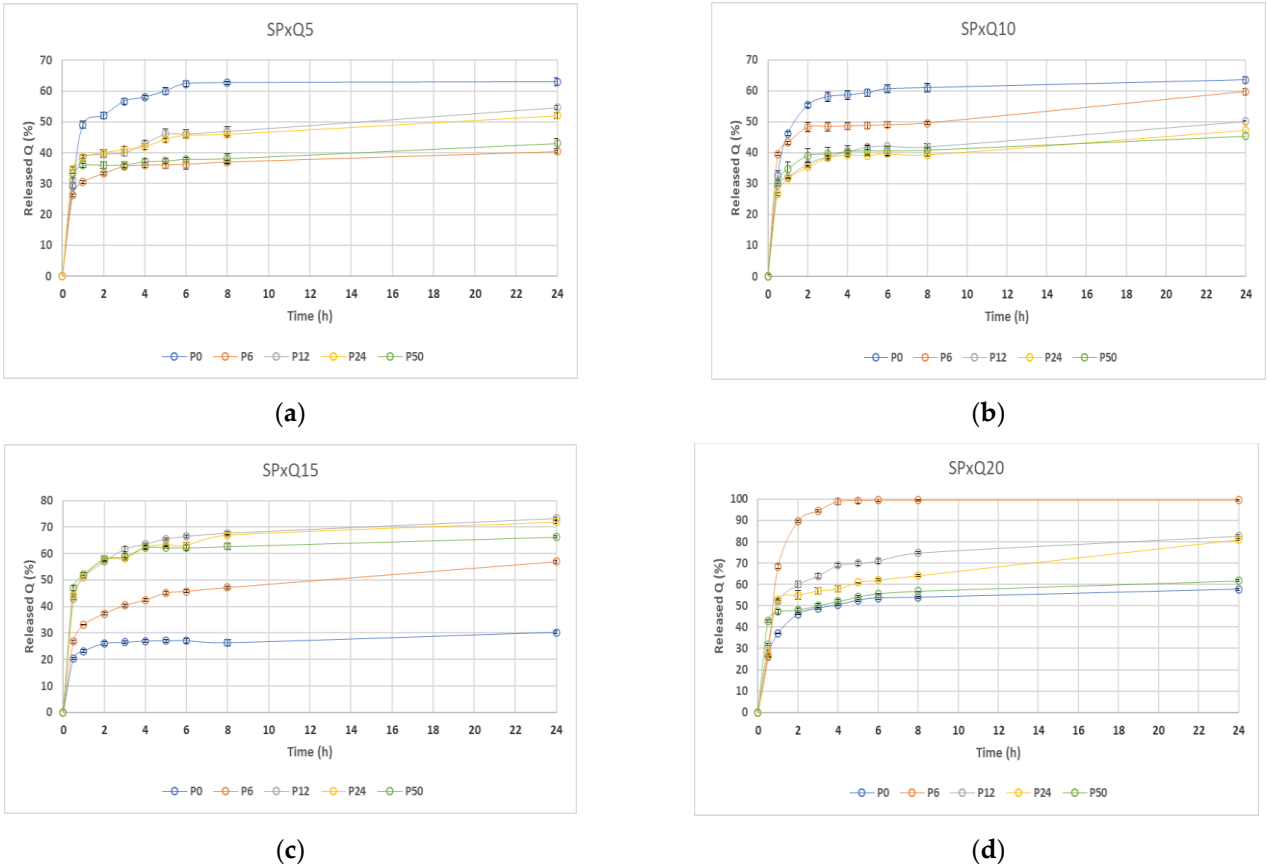

Figure 11. Release of quercetin in function of the P percentage and with (**a**) 5 wt% of Q, (**b**) 10 wt% of Q, (**c**) 15 wt% of Q, and (**d**) 20 wt% of Q.

When P is absent in the system, approximately 50% of the quercetin present is released after about 1 h. During the following hours, the release of quercetin increases until reaching, after about 6 h, an overall release of about 63%, which remains constant over time, up to the monitored 24 h. When P is added to the system, regardless of the amount of P added, the release always reaches lower percentages, and the trend appears slower and more controlled. Quercetin, thanks to the presence in its structure of -OH and C=O groups, is able to form both hydrophobic bonds with other quercetins and hydrogen bonds with the -OH groups of the sol–gel matrix [59–61]. When the amount of quercetin in the system is low, the probability of quercetin–quercetin hydrophobic bonds decreases, so most of the interactions are hydrogen bonding with the SiO_2 network (Figure 11a). However, these interactions are weak and in solution, they tend to break down, thus leading to the release of most of the quercetin. When P is added to the system, the possible interactions that can occur increase, and P can interact with both the SiO_2 matrix and quercetin [38,60]. In this type of system, Q could in any case bind to the SiO_2 matrix and to P, the latter being constituted of long chains that might entrap the quercetin, which would therefore no longer be released (Figure 11b). This hypothesis could explain why, at low quantities of quercetin, the system in which the polyethylene glycol is present favors slow and sustained release over time in comparison to the system without P.

This reasoning also seems to be consistent with the SQ10 and SP(6–50)Q10 systems; however, the trend was not found in the SQ(15 and 20 wt%) and SP(6–50 wt%)Q(15 and 20 wt%) systems. In these cases, in fact, the release is lower when P is absent and higher when P is added. In this scenario, the hypothesis is that an increase in the amount of quercetin within the system enhances the likelihood of greater interaction between quercetin molecules through hydrophobic bonds. These quercetin clusters could therefore remain blocked in the SiO_2 matrix and consequently not be available for release in solution

(Figure 11c). On the contrary, when P is added to the system, it may interact with the sol–gel network through its long chains, which could hamper the trapping, which in the absence of P, would lead to quercetin clusters inside the SiO_2 matrix. Consequently, quercetin would be linked in part with itself, in part with the network, and in part with P through hydrogen bonds (Figure 11d). All these hypotheses are depicted in Figure 12.

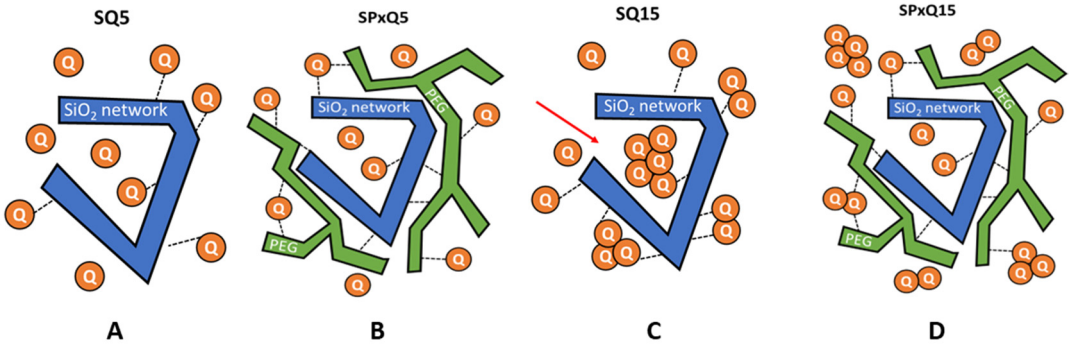

Figure 12. Possible mechanisms of release of high and low percentage of quercetin, with and without P. (**A**) SQ5 system; (**B**) SPxQ5 system; (**C**) SQ15 and (**D**) SPxQ15 systems.

4. Conclusions

The sol–gel method was employed in this study to synthesize hybrid materials incorporating silica (S), polyethylene glycol (P), and quercetin (Q). Different percentages of P and Q were incorporated into the silica matrix to investigate their influence on the properties of the materials. The synthesized materials were characterized using FT-IR analysis and solid-state NMR spectroscopy, and their in vitro release behavior was evaluated.

Insights into the interactions between the organic and inorganic components within the hybrids were obtained through the deconvolution of the main absorption band, as observed in the FT-IR analysis. The spectra revealed the presence of characteristic absorption bands corresponding to S, P, and Q. The shifts in absorption bands and the appearance of new peaks indicated the influence of the polyethylene glycol and quercetin on the silica matrix. Moreover, the shifts in Si-O-Si skeletal vibrations and the appearance of C-O-C aryl ketone vibrations suggested the interaction between the organic phases and the silica matrix. These results support the hypothesis of interactions between all the components inside the hybrid materials.

Furthermore, solid-state NMR analysis confirmed the presence of P and Q in the hybrid systems. Indeed, the NMR spectra showed distinct peaks corresponding to the chemical shifts of P and Q, indicating their successful incorporation into the silica matrix. The condensation degree of silica in the composites was also assessed, providing valuable information about the structure of the materials.

The in vitro release study highlights how the presence or absence of P (polyethylene glycol) has notable influences on the properties, specifically on the release behavior, of quercetin. In particular, the presence of P plays a vital role in restricting the movement of quercetin, leading to a slower release profile. Due to its configuration, P physically entraps Q inside the S matrix and interacts with quercetin by H-bonds, thus reducing its mobility and impeding diffusion out of the SP matrix.

Thus, the results indicate that the SPQ-synthesized materials exhibited controlled release properties, suggesting their potential application in drug-delivery systems.

Author Contributions: Conceptualization, M.C. and P.M.; methodology, V.P., V.V. and A.D.; validation, V.P., V.V. and A.D.; formal analysis, A.D. and M.M.D.; investigation, V.P., V.V. and A.D.; resources, M.C. and P.M.; data curation, V.P., V.V. and A.D.; writing—original draft preparation, M.C., P.M. and A.D.; writing—review and editing, M.C.; P.M. and M.M.D.; visualization, V.P., V.V. and A.D.; supervision, M.C. and P.M.; project administration, M.C. and P.M. All authors have read and agreed to the published version of the manuscript.

Funding: This research received no external funding.

Institutional Review Board Statement: Not applicable.

Informed Consent Statement: Not applicable.

Data Availability Statement: The data presented in this study are available on request from the corresponding author.

Acknowledgments: This work was supported in part by "SCAVENGE", financed by Università degli Studi della Campania Luigi Vanvitelli in the framework of "Piano Strategico di Ateneo 2021–2023—Azione strategica R1.S2".

Conflicts of Interest: The authors declare no conflict of interest.

References

1. Maleki, A. (Ed.) *Heterogeneous Micro and Nanoscale Composites for the Catalysis of Organic Reactions*; Elsevier: Amsterdam, The Netherlands, 2022; ISBN 978-0-323-85289-0.
2. Kickelbick, G. Hybrid Materials—Past, Present and Future. *Hybrid Mater.* **2014**, *1*, 39–51. [CrossRef]
3. Saleh, T.A. Hybrid Materials: Fundamentals and Classifications. In *Polymer Hybrid Materials and Nanocomposites*; Elsevier: Amsterdam, The Netherlands, 2021; pp. 147–176. ISBN 978-0-12-813294-4.
4. Vallet-Regí, M.; Colilla, M.; González, B. Medical Applications of Organic–Inorganic Hybrid Materials within the Field of Silica-Based Bioceramics. *Chem. Soc. Rev.* **2011**, *40*, 596–607. [CrossRef]
5. Arcos, D.; Vallet-Regí, M. Sol–Gel Silica-Based Biomaterials and Bone Tissue Regeneration. *Acta Biomater.* **2010**, *6*, 2874–2888. [CrossRef]
6. Fernández-Hernán, J.P.; Torres, B.; López, A.J.; Rams, J. The Role of the Sol-Gel Synthesis Process in the Biomedical Field and Its Use to Enhance the Performance of Bioabsorbable Magnesium Implants. *Gels* **2022**, *8*, 426. [CrossRef]
7. Hong, G.S.; Choi, J.Y.; Suh, J.S.; Lim, J.O.; Choi, J.H. Development of a Natural Matrix Hybrid Hydrogel Patch and Evaluation of Its Efficacy against Atopic Dermatitis. *Appl. Sci.* **2020**, *10*, 8759. [CrossRef]
8. Valentino, A.; Di Cristo, F.; Bosetti, M.; Amaghnouje, A.; Bousta, D.; Conte, R.; Calarco, A. Bioactivity and Delivery Strategies of Phytochemical Compounds in Bone Tissue Regeneration. *Appl. Sci.* **2021**, *11*, 5122. [CrossRef]
9. Francenia Santos-Sánchez, N.; Salas-Coronado, R.; Villanueva-Cañongo, C.; Hernández-Carlos, B. Antioxidant Compounds and Their Antioxidant Mechanism. In *Antioxidants*; Shalaby, E., Ed.; IntechOpen: London, UK, 2019; ISBN 978-1-78923-919-5.
10. Lobo, V.; Patil, A.; Phatak, A.; Chandra, N. Free Radicals, Antioxidants and Functional Foods: Impact on Human Health. *Pharmacogn. Rev.* **2010**, *4*, 118–126. [CrossRef]
11. Martemucci, G.; Costagliola, C.; Mariano, M.; D'andrea, L.; Napolitano, P.; D'Alessandro, A.G. Free Radical Properties, Source and Targets, Antioxidant Consumption and Health. *Oxygen* **2022**, *2*, 48–78. [CrossRef]
12. Pham-Huy, L.A.; He, H.; Pham-Huy, C. Free Radicals, Antioxidants in Disease and Health. *Int. J. Biomed. Sci.* **2008**, *4*, 89–96. [PubMed]
13. Di Meo, S.; Venditti, P. Evolution of the Knowledge of Free Radicals and Other Oxidants. *Oxidative Med. Cell. Longev.* **2020**, *2020*, 9829176. [CrossRef]
14. Azat Aziz, M.; Shehab Diab, A.; Abdulrazak Mohammed, A. Antioxidant Categories and Mode of Action. In *Antioxidants*; Shalaby, E., Ed.; IntechOpen: London, UK, 2019; ISBN 978-1-78923-919-5.
15. Gonçalves, A.C.; Nunes, A.R.; Meirinho, S.; Ayuso-Calles, M.; Roca-Couso, R.; Rivas, R.; Falcão, A.; Alves, G.; Silva, L.R.; Flores-Félix, J.D. Exploring the Antioxidant, Antidiabetic, and Antimicrobial Capacity of Phenolics from Blueberries and Sweet Cherries. *Appl. Sci.* **2023**, *13*, 6348. [CrossRef]
16. Zhang, M.; Swarts, S.G.; Yin, L.; Liu, C.; Tian, Y.; Cao, Y.; Swarts, M.; Yang, S.; Zhang, S.B.; Zhang, K.; et al. Antioxidant Properties of Quercetin. In *Oxygen Transport to Tissue XXXII.*; LaManna, J.C., Puchowicz, M.A., Xu, K., Harrison, D.K., Bruley, D.F., Eds.; Advances in Experimental Medicine and Biology; Springer: Boston, MA, USA, 2011; Volume 701, pp. 283–289. ISBN 978-1-4419-7755-7.
17. Anand David, A.; Arulmoli, R.; Parasuraman, S. Overviews of Biological Importance of Quercetin: A Bioactive Flavonoid. *Pharmacogn. Rev.* **2016**, *10*, 84–89. [CrossRef]
18. Li, Y.; Yao, J.; Han, C.; Yang, J.; Chaudhry, M.; Wang, S.; Liu, H.; Yin, Y. Quercetin, Inflammation and Immunity. *Nutrients* **2016**, *8*, 167. [CrossRef] [PubMed]
19. Vergara-Castañeda, H.; Hernandez-Martinez, A.R.; Estevez, M.; Mendoza, S.; Luna-Barcenas, G.; Pool, H. Quercetin Conjugated Silica Particles as Novel Biofunctional Hybrid Materials for Biological Applications. *J. Colloid Interface Sci.* **2016**, *466*, 44–55. [CrossRef]
20. Lee, G.H.; Lee, S.J.; Jeong, S.W.; Kim, H.-C.; Park, G.Y.; Lee, S.G.; Choi, J.H. Antioxidative and Antiinflammatory Activities of Quercetin-Loaded Silica Nanoparticles. *Colloids Surf. B Biointerfaces* **2016**, *143*, 511–517. [CrossRef] [PubMed]
21. Catauro, M.; Tranquillo, E.; Salzillo, A.; Capasso, L.; Illiano, M.; Sapio, L.; Naviglio, S. Silica/Polyethylene Glycol Hybrid Materials Prepared by a Sol-Gel Method and Containing Chlorogenic Acid. *Molecules* **2018**, *23*, 2447. [CrossRef]

22. Oubaha, M. Introduction to Hybrid Sol-Gel Materials. In *World Scientific Series in Nanoscience and Nanotechnology*; World Scientific: Singapore, 2019; Volume 3, pp. 1–36. ISBN 978-981-327-055-8.
23. Catauro, M.; Bollino, F.; Papale, F.; Gallicchio, M.; Pacifico, S. Influence of the Polymer Amount on Bioactivity and Biocompatibility of SiO_2/PEG Hybrid Materials Synthesized by Sol–Gel Technique. *Mater. Sci. Eng. C* **2015**, *48*, 548–555. [CrossRef] [PubMed]
24. Catauro, M.; D'Angelo, A.; Fiorentino, M.; Pacifico, S.; Latini, A.; Brutti, S.; Vecchio Ciprioti, S. Thermal, Spectroscopic Characterization and Evaluation of Antibacterial and Cytotoxicity Properties of Quercetin-PEG-Silica Hybrid Materials. *Ceram. Int.* **2023**, *49*, 14855–14863. [CrossRef]
25. Manna, A.; Pramanik, S.; Tripathy, A.; Moradi, A.; Radzi, Z.; Pingguan-Murphy, B.; Hasnand, N.; Abu Osman, N.A. Development of biocompatible hydroxyapatite–poly(ethylene glycol) core–shell nanoparticles as an improved drug carrier: Structural and electrical characterizations. *RSC Adv.* **2016**, *6*, 102853–102868. [CrossRef]
26. Bossard, C.; Granel, H.; Wittrant, Y.; Jallot, É.; Lao, J.; Vial, C.; Tiainen, H. Polycaprolactone/bioactive glass hybrid scaffolds for bone regeneration. *Biomed. Glas.* **2018**, *4*, 108–122. [CrossRef]
27. Bokov, D.; Turki Jalil, A.; Chupradit, S.; Suksatan, W.; Javed Ansari, M.; Shewael, I.H.; Valiev, G.H.; Kianfar, E. Nanomaterial by Sol-Gel Method: Synthesis and Application. *Adv. Mater. Sci. Eng.* **2021**, *2021*, 5102014. [CrossRef]
28. Chakraborty, P.K.; Adhikari, J.; Saha, P. Variation of the Properties of Sol–Gel Synthesized Bioactive Glass 45S5 in Organic and Inorganic Acid Catalysts. *Mater. Adv.* **2021**, *2*, 413–425. [CrossRef]
29. Brinker, C.J.; Scherer, G.W. *Sol-Gel Science: The Physics and Chemistry of Sol-Gel Processing*; Academic Press, Inc.: Boston, MA, USA, 1990; ISBN 9780121349707.
30. Danks, A.E.; Hall, S.R.; Schnepp, Z. The Evolution of 'Sol–Gel' Chemistry as a Technique for Materials Synthesis. *Mater. Horiz.* **2016**, *3*, 91–112. [CrossRef]
31. Colleoni, C.; Esposito, S.; Grasso, R.; Gulino, M.; Musumeci, F.; Romeli, R.; Rosace, G.; Salesi, G.; Scordino, A. Delayed luminescence induced by complex domains in water and in aqueous solutions. *Chem. Phys.* **2016**, *18*, 772–780. [CrossRef]
32. Spěváček, J.; Baldrian, J. Solid-State ^{13}C NMR and SAXS Characterization of the Amorphous Phase in Low-Molecular Weight Poly(Ethylene Oxide)s. *Eur. Polym. J.* **2008**, *44*, 4146–4150. [CrossRef]
33. Geppi, M.; Mollica, G.; Borsacchi, S.; Marini, M.; Toselli, M.; Pilati, F. Solid-State Nuclear Magnetic Resonance Characterization of PE–PEG/Silica Hybrid Materials Prepared by Microwave-Assisted Sol-Gel Process. *J. Mater. Res.* **2007**, *22*, 3516–3525. [CrossRef]
34. Srinivasan, A.; Nallaiyan, R. Surface characteristics, corrosion resistance and MG63 osteoblast-like cells attachment behaviour of nano SiO_2–ZrO_2 coated 316L stainless steel. *RSC Adv.* **2015**, *5*, 26007–26016. [CrossRef]
35. Kokubo, T.; Kushitani, H.; Sakka, S.; Kitsugi, T.; Yamamuro, T. Solutions Able to Reproduce In Vivo Surface-Structure Changes in Bioactive Glass-Ceramic A-W3. *J. Biomed. Mater. Res.* **1990**, *24*, 721–734. [CrossRef] [PubMed]
36. Kokubo, T.; Takadama, H. How Useful Is SBF in Predicting In Vivo Bone Bioactivity? *Biomaterials* **2006**, *27*, 2907–2915. [CrossRef]
37. Catauro, M.; D'Angelo, A.; Fiorentino, M.; Gullifa, G.; Risoluti, R.; Vecchio Ciprioti, S. Thermal Behavior, Morphology and Antibacterial Properties Study of Silica/Quercetin Nanocomposite Materials Prepared by Sol–Gel Route. *J. Therm. Anal. Calorim.* **2021**, *147*, 5337–5350. [CrossRef]
38. Blanco, I.; Latteri, A.; Cicala, G.; D'Angelo, A.; Viola, V.; Arconati, V.; Catauro, M. Antibacterial and Chemical Characterization of Silica-Quercetin-PEG Hybrid Materials Synthesized by Sol–Gel Route. *Molecules* **2022**, *27*, 979. [CrossRef] [PubMed]
39. Zenkevich, I.G.; Eshchenko, A.Y.; Makarova, S.V.; Vitenberg, A.G.; Dobryakov, Y.G.; Utsal, V.A. Identification of the Products of Oxidation of Quercetin by Air Oxygenat Ambient Temperature. *Molecules* **2007**, *12*, 654–672. [CrossRef]
40. Fuentes, J.; Atala, E.; Pastene, E.; Carrasco-Pozo, C.; Speisky, H. Quercetin Oxidation Paradoxically Enhances its Antioxidant and Cytoprotective Properties. *J. Agric. Food Chem.* **2017**, *65*, 11002–11010. [CrossRef]
41. Doroshenko, I.; Pogorelov, V.; Sablinskas, V. Infrared Absorption Spectra of Monohydric Alcohols. *Dataset Pap. Chem.* **2013**, *2013*, 329406. [CrossRef]
42. Innocenzi, P. Infrared Spectroscopy of Sol–Gel Derived Silica-Based Films: A Spectra-Microstructure Overview. *J. Non-Cryst. Solids* **2003**, *316*, 309–319. [CrossRef]
43. Fidalgo, A.; Ilharco, L.M. The Defect Structure of Sol–Gel-Derived Silica/Polytetrahydrofuran Hybrid Films by FTIR. *J. Non-Cryst. Solids* **2001**, *283*, 144–154. [CrossRef]
44. Ellerbrock, R.; Stein, M.; Schaller, J. Comparing Amorphous Silica, Short-Range-Ordered Silicates and Silicic Acid Species by FTIR. *Sci. Rep.* **2022**, *12*, 11708. [CrossRef] [PubMed]
45. Al-Oweini, R.; El-Rassy, H. Synthesis and Characterization by FTIR Spectroscopy of Silica Aerogels Prepared Using Several $Si(OR)_4$ and $R''Si(OR')_3$ Precursors. *J. Mol. Struct.* **2009**, *919*, 140–145. [CrossRef]
46. Capeletti, L.B.; Zimnoch, J.H. Fourier Transform Infrared and Raman Characterization of Silica-Based Materials. In *Applications of Molecular Spectroscopy to Current Research in the Chemical and Biological Sciences*; Stauffer, M.T., Ed.; InTech: London, UK, 2016; ISBN 978-953-51-2680-5.
47. Almeida, R.M.; Pantano, C.G. Structural Investigation of Silica Gel Films by Infrared Spectroscopy. *J. Appl. Phys.* **1990**, *68*, 4225–4232. [CrossRef]
48. Syabani, M.W.; Rochmadi, R.; Perdana, I.; Prasetya, A. FTIR Study on Nano-Silica Synthesized from Geothermal Sludge. In Proceedings of the 4th International Conference on Materials Engineering and Nanotechnology (ICMEN 2021), Kuala Lumpur, Malaysia, 3–4 April 2021; p. 030014.

49. Chakraborty, S.; Biswas, S.; Sa, B.; Das, S.; Dey, R. In Vitro & In Vivo Correlation of Release Behavior of Andrographolide from Silica and PEG Assisted Silica Gel Matrix. *Colloids Surf. A Physicochem. Eng. Asp.* **2014**, *455*, 111–121. [CrossRef]
50. Khairuddin; Pramono, E.; Utomo, S.B.; Wulandari, V.; Zahrotul, W.A.; Clegg, F. FTIR Studies on the Effect of Concentration of Polyethylene Glycol on Polimerization of Shellac. *J. Phys. Conf. Ser.* **2016**, *776*, 012053. [CrossRef]
51. Wu, H.; Huang, S.; Jiang, Z. Effects of Modification of Silica Gel and ADH on Enzyme Activity for Enzymatic Conversion of CO_2 to Methanol. *Catal. Today* **2004**, *98*, 545–552. [CrossRef]
52. Vrandečić, N.S.; Erceg, M.; Jakić, M.; Klarić, I. Kinetic Analysis of Thermal Degradation of Poly(Ethylene Glycol) and Poly(Ethylene Oxide)s of Different Molecular Weight. *Thermochim. Acta* **2010**, *498*, 71–80. [CrossRef]
53. Shameli, K.; Bin Ahmad, M.; Jazayeri, S.D.; Sedaghat, S.; Shabanzadeh, P.; Jahangirian, H.; Mahdavi, M.; Abdollahi, Y. Synthesis and Characterization of Polyethylene Glycol Mediated Silver Nanoparticles by the Green Method. *Int. J. Mol. Sci.* **2012**, *13*, 6639–6650. [CrossRef]
54. Porto, I.C.C.M.; Nascimento, T.G.; Oliveira, J.M.S.; Freitas, P.H.; Haimeur, A.; França, R. Use of Polyphenols as a Strategy to Prevent Bond Degradation in the Dentin-Resin Interface. *Eur. J. Oral Sci.* **2018**, *126*, 146–158. [CrossRef]
55. Wang, Q.; Wei, H.; Deng, C.; Xie, C.; Huang, M.; Zheng, F. Improving Stability and Accessibility of Quercetin in Olive Oil-in-Soy Protein Isolate/Pectin Stabilized O/W Emulsion. *Foods* **2020**, *9*, 123. [CrossRef] [PubMed]
56. Khawory, M.H.; Subki, M.F.M.; Shahudin, M.A.; Sofian, N.H.A.S.; Latif, N.H.; Salin, N.H.; Zobir, S.Z.M.; Noordin, M.I. Physico-Chemicals Characterization of Quercetin from the *Carica papaya* Leaves by Different Extraction Techniques. *Open J. Phys. Chem.* **2021**, *11*, 129–143. [CrossRef]
57. Silverstein, R.M.; Bassler, G.C. Spectrometric Identification of Organic Compounds. *J. Chem. Educ.* **1962**, *39*, 546. [CrossRef]
58. Speisky, H.; Arias-Santé, M.F.; Fuentes, J. Oxidation of Quercetin and Kaempferol Markedly Amplifies Their Antioxidant, Cytoprotective, and Anti-Inflammatory Properties. *Antioxidants* **2023**, *12*, 155. [CrossRef] [PubMed]
59. Formica, J.V.; Regelson, W. Review of the biology of quercetin and related bioflavonoids. *Food Chem. Toxicol.* **1995**, *33*, 1061–1080. [CrossRef]
60. Catauro, M.; Bollino, F.; Gloria, A. Sol-Gel Synthesis and Characterization of SiO_2/PEG Hybrid Materials Containing Quercetin as Implants with Antioxidant Properties. *AIP Conf. Proceeding* **2016**, *1736*, 20096. [CrossRef]
61. Raffaini, G.; Catauro, M. Surface Interactions between Ketoprofen and Silica-Based Biomaterials as Drug Delivery System Synthesized via Sol–Gel: A Molecular Dynamics Study. *Materials* **2022**, *15*, 2759. [CrossRef] [PubMed]